Annals of Nuclear Energy 113 (2018) 177–193

Contents lists available at ScienceDirect

Annals of Nuclear Energy

journal homepage: www.elsevier.com/locate/anucene

Nonlinear dynamic model of Molten-Salt Reactor Experiment – Validation and operational analysis

Vikram Singh *, Alexander M. Wheeler, Matthew R. Lish, Ondřej Chvála, Belle R. Upadhyaya

University of Tennessee, Department of Nuclear Engineering, Knoxville, TN 37996-2300, United States

ARTICLE INFO

Article history:
Received 25 August 2017
Accepted 27 October 2017
Available online 21 November 2017

Keywords:
MSRE
Dynamic modeling
Validation
Parameters
Operational anomaly
Transient response
Frequency response
Pump-trip
Cold-slug

ABSTRACT

Several molten-salt reactor (MSR) concepts are currently being developed by private vendors and national organizations. Molten-Salt Reactor Experiment (MSRE) is the only MSR that operated for several years, for which the performance was well documented in the literature. Experimental data from MSRE serve as the standard for developing models and tools for MSR analysis. MSRE underwent several design changes from conception to construction to operation. Model validation requires the use of parameters consistent with those that existed during the various measurements. The paper therefore presents a brief discussion of the parameters that evolved over time, and details of sources for all the parameters used in the modeling. This report is part of a series of papers on modeling MSR dynamics. The goal here is to validate the modeling approach by comparing simulation results with experimental data. For this purpose, two nonlinear dynamic models are developed. The first model uses a one-region one-dimensional representation of the core. The second reproduces the nine-region core model developed by Oak Ridge National Laboratory for MSRE studies. The dynamics are analyzed by simulating transients during normal power operation. The frequency response of the models is also evaluated. Both models show excellent agreement with experimental data for both U-235 and U-233 fuels. Some apparent discrepancies in experimental data are reported and their consequences discussed. The one-region model is modified to simulate reactivity excursions resulting from operational anomalies, and the results are presented. This modeling approach can be applied to other MSR systems provided valid system parameters.

1. Introduction

The Molten-Salt Reactor Program (MSRP) was conducted at Oak Ridge National Laboratory (ORNL) from 1958 to 1976. The objective of the program was to develop liquid fuel nuclear reactors that used solutions of fissile or fertile material in suitable carrier salts as both fuel and primary coolant. An essential goal of the program was to use the thorium cycle and to extend fuel resources (McNeese, 1976).

A significant achievement of the MSRP was the design, construction, and operation of the Molten-Salt Reactor Experiment (MSRE) (Haubenreich and Engel, 1970). MSRE was an 8 MW(th) reactor with an operating temperature of ~650 °C. A liquid fuel salt circulated through an external pump into the reactor core containing graphite blocks for neutron moderation. The fuel salt then flowed through a salt-salt heat exchanger. The secondary circuit comprised of a molten salt with comparable properties but without any actinides. It circulated through a radiator to dissipate the heat to the atmosphere. The primary and the secondary circuits were made of INOR-8, a nickel-molybdenum-iron-chromium alloy.[1] The purpose of MSRE was to demonstrate the reliability of critical components and develop components and other technology necessary for a commercial molten-salt reactor demonstration. It was the first reactor ever primarily to operate using U-233 fuel.

Experiments carried out at MSRE showed the practicality of handling molten salts in an operating reactor. The salt chemistry was found to behave well at the elevated temperature and high radiation environment with minimal corrosion in both the graphite and INOR-8 components. The reactor's dynamic behavior correlated well with predictions as reported by Kerlin et al. (1971a). Radioactive core component maintenance was accomplished with little exposure, and xenon was removed in the pump bowl by gas sparging. MSRE had many instruments installed for characterization of reactor operation. System monitoring was mainly accomplished using more than 1000 type-K thermocouples that measured temperature in various flow regions of the reactor system (Robertson, 1965). The second phase of the program aimed at reprocessing

* Corresponding author.
E-mail address: vsingh10@vols.utk.edu (V. Singh).

[1] Currently available under commercial trademark Hastelloy®-N.

https://doi.org/10.1016/j.anucene.2017.10.047
0306-4549/

the molten fluoride salts was carried out, and uranium along with fission products such as tellurium, iodine, niobium, molybdenum etc. were recovered (Lindauer, 1969). MSRE operation ended in 1969 and the program was permanently shut down in 1973 citing budgetary reasons (Rosenthal, 2009). MSRE is the only example of a well-characterized, power-operated molten-salt reactor (MSR). Therefore, its results serve as benchmarks for current MSR studies. Before the conclusion of the MSRP in 1976, several studies were carried out on molten-salt breeder reactor (MSBR) designs. Efforts were devoted to technology development needed for full-scale molten-salt reactor demonstrations including studies on materials, fuel and coolant salt chemistry, fission-product behavior, processing methods, and systems and components development. These results were documented in hundreds of reports and peer-reviewed publications. A world wide web repository of many of these papers can be found at Ref. Documents.

MSRs operate at an elevated temperature of ~700 °C and ambient pressures, thus enabling improved thermodynamic conversion efficiency. The lack of need for a pressurized containment both reduces cost and improves safety as compared to light water reactors (LWR). The liquid fuel core provides a passively safe design and an overall negative prompt reactivity coefficient. Continuously online fuel reprocessing can efficiently extract fission products of interest. These features make MSRs an attractive Generation-IV technology.

The design study presented in this paper is part of a series of work on modeling the dynamic characteristics of MSRs. As part of the project, dynamic models were developed for the MSRE and a two-fluid MSBR to study time-dependent behavior under reactivity excursions, proposed control strategies, and credible operational anomaly scenarios (Singh et al., 2017a,b).

This paper focuses on comparing simulation results with experimental data obtained during the operation of the MSRE. It presents two nonlinear dynamic models built for this purpose. The first model uses one region to describe the core. The second model uses nine such regions each with a weighted power distribution to conveniently reproduce the theoretical model published by ORNL, (Kerlin et al., 1971b). Details of model development along with validation of the modeling approach are the primary topics of discussion. This paper also presents results from the simulation of credible operational anomalies using the one-region model. In the context of this modeling study, some effort was devoted to assembling a consistent set of parameters for the MSRE modeling from a vast catalog of information acquired from a decade of MSRE development and operation. The paper discusses this process and lists parameters of interest. The nodal models for the MSRE described here are an extension of the model described in Singh et al. (2017a), and evaluation of results will serve to validate the modeling approach (Singh et al., 2017b).

The developed nonlinear nodal models are an attempt to reflect the MSRE design accurately. In doing so, the models simulate the dynamic behavior of the neutron kinetics, heat transfer, and fluid transport. The only difference is that the nine-region model distributes the total power generated and the associated temperature changes among the nine core regions using appropriate importance factors. The one-region model assumes uniform temperature effects in the core. This paper compares the results of simulation for both the developed models against experimental data for time response and frequency response of the system to reactivity insertions and elaborates on the main observations. This paper also discusses modifications to the one-region model to allow simulation of conceivable operational anomalies and their resulting reactivity transients and presents the simulation results.

The contained information is organized as follows: A brief overview of the timeline of the MSRE operation and the description of the reactor system is presented in Section 2. The development of both the one-region and nine-region models along with modifications to the one-region model for simulating incidents, modeling parameters, and model equations are described in Section 3. The results of simulation and comparisons with experimental data are presented in Section 4. Finally, the main conclusions derived from the study are outlined in Section 5.

2. Description of the system

This section discusses the general features and characteristics of the MSRE system. The information is arranged as follows. Section 2.1 provides a brief discussion of the timeline of operation of MSRE, followed by a description of the reactor system, its dynamic characteristics and the effect of fuel types in Section 2.2. The main intention here is to provide a sufficient background to develop the dynamic models presented in Section 3.

2.1. Brief timeline of MSRE operation

The MSRE operated from June 1965 through December 1969. The design of the MSRE began in the summer of 1960 with the fabrication of INOR-8 and graphite components following in the years after. Installation of the systems finished in the summer of 1964, followed by pre-critical tests to determine the functionality of all systems. Meanwhile, the design and operation reports and dynamics studies were published (Robertson, 1965; Haubenreich et al., 1964).

The carrier salt circulated in the final pre-critical tests contained depleted uranium that was enriched with 61 wt% UF_4-LiF eutectic salt, and the MSRE went critical on June 1, 1965 (Haubenreich and Engel, 1970). It operated at zero-power for a few months while control rod calibration and measurement of reactivity coefficients needed for future analysis were carried out. Tests in the kilowatt range showed that the dynamics of the system behaved as expected. In the approach to full power, the reactor was operated at several intermediate power levels to observe its dynamics, xenon behavior, and fuel chemistry. MSRE was designed to be a 10 MW(th) reactor, although in the final stages of power escalation it was discovered that the heat extraction in the secondary system was smaller than expected. Therefore, the maximum steady-state power level was restricted to ~7.2 MW, as measured from heat balances (Haubenreich and Engel, 1970). Later, the coolant salt specific heat was measured and found to be 11% higher than the original value. Hence MSRE operated at close to 8 MW. Full power operation with U-235 fuel continued until 1968, with short interruptions for maintenance and components inspections.

Operation with U-235 fuel ended in March 1968, followed by several months of preparations to strip the uranium from the carrier salt by a fluoride volatility process, and replace it with U-233. Fluorination of the fuel salt recovered the 218 kg of uranium with 47 h of fluorine sparging over a 6-day period. Corrosion products were reduced and filtered in another ten days. MSRE again went critical in October of 1968, but this time with U-233 fuel, making it the first reactor ever operated primarily on this fuel type. Following a set of zero-power physics experiments, the reactor was stepped up to 1, 5, and 8 MW with dynamics tests and observations of reactivity and radiation heating at each level (Haubenreich and Engel, 1970). As was expected, MSRE was found to be operationally stable over the entire range of power, with the dynamic characteristics showing close agreement with predictions for both U-233 and U-235 fuel loadings.

2.2. Description of the MSRE system

MSRE was an experimental reactor and detailed studies of its dynamic characteristics were performed prior to both U-235 and

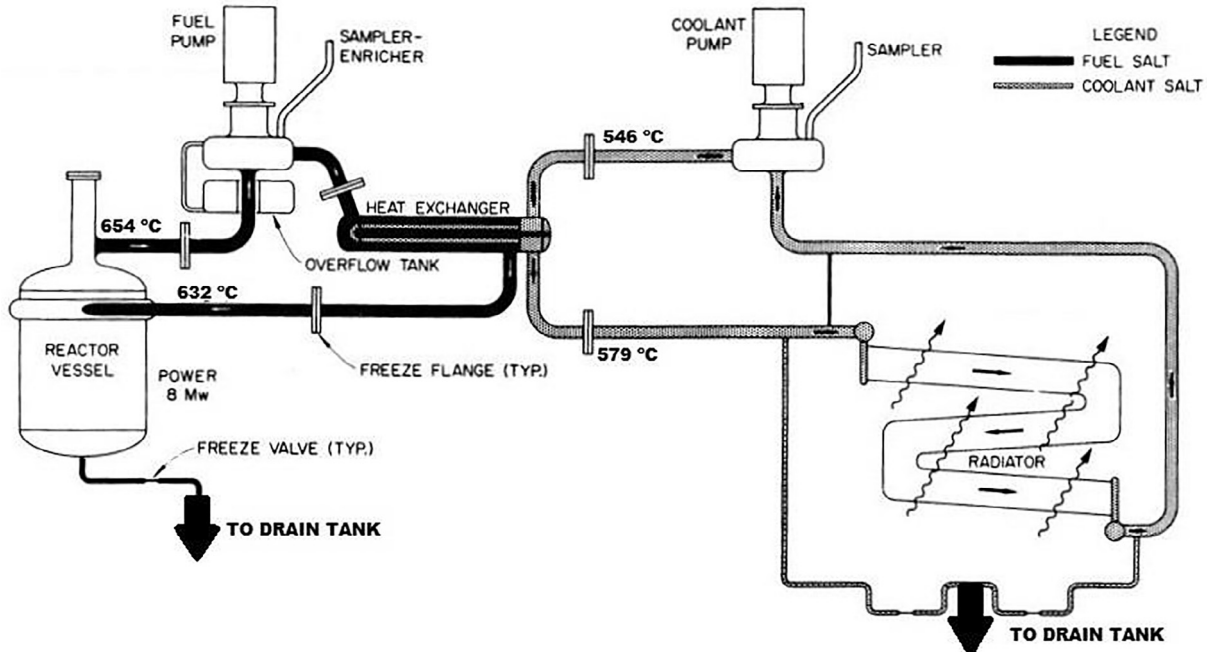

Fig. 1. Simplified schematic of the Molten-Salt Reactor Experiment (MSRE) system. Temperatures changed to degrees Celsius. Source: Kerlin et al.(1971a), © Nuclear Technology.

U-233 fuel loading. Fig. 1 shows a simplified schematic of the MSRE. The core was composed of a matrix of rectangular graphite blocks for neutron moderation. The graphite blocks were coated with pyrolytic carbon to reduce permeability. Grooves on the sides of the graphite blocks formed channels for the fluid fuel to flow up through the graphite lattice. The molten, fuel-bearing carrier salt of ^{7}LiF-BeF_2-ZrF_4-UF_4 (65–29.1–5-0.9 mol%) at 632 °C was pumped through the core where the 8 MW of heat generated through fission raised the temperature of the salt by ~22 °C. The fuel salt then circulated through a heat exchanger where it transferred the primary heat to a non-fueled secondary coolant salt of ^{7}LiF-BeF_2 (66–34 mol%) before returning to the core. The secondary coolant salt circulated through an air-cooled radiator and rejected heat to the atmosphere.

All other salt-containing components were constructed from INOR-8. Three flexible control rods consisting of gadolinium in the form of Gd2O3-Al2O3 ceramic clad with Inconel were driven on a chain and clutch system to raise and lower the rods. The negative reactivity coefficient of the reactor system along with low excess reactivity meant that nuclear safety was not primarily dependent on fast moving control rods. The rods were used to maintain power level and outlet fuel temperature.

Criticality in MSRE was first achieved with U-235 fuel (33% enriched). After 9006 equivalent full power hours of operation, the reactor was refueled with U-233 (91% enriched) for an additional 4166 equivalent full power hours of operation (Haubenreich and Engel, 1970). Extensive theoretical studies were carried out prior to the functioning of the reactor. As mentioned before, the reactor was operated at different power levels from zero-power to full power of 8 MW(th) during the experiment to make measurements and study stability at all power levels. This was true for both U-235 and U-233 operation.

The product of mass flow rate of the salt, specific heat capacity (at constant pressure), and the difference in the inlet and outlet temperatures of the salt gives the power generated in the system. This measurement was made using thermocouples placed on the outside of piping in the secondary system. The flow rate of the salt streams is not meant to change in MSRE. Hence, only the temperature difference between the inlet and outlet salt changes during operation at different power levels.

The two most important characteristics of MSRE that contribute to the dynamic behavior are its heterogeneous core and its fluid fuel that circulates continuously. The fuel circulation reduces the delayed-neutron precursors decaying in the core, reduces the rate of temperature change in the fuel during a power change, and introduces delayed fuel-temperature and neutron-production effects. The heterogeneity of the core induces delayed feedback effects due to slow temperature variations in the graphite (Kerlin et al., 1971b). The main difference in the two fissile fuel types used at MSRE and considered here are the relative delayed-neutron fractions. U-233 has a total delayed neutron fraction, β, of 0.00264 as opposed to 0.0065 for U-235. Also, temperature changes in the salt have a much larger effect on the reactivity feedback than temperature variations in the graphite. The heat transfer and heat capacities of the core components are such that rapid changes in temperature of the fuel salt do not translate to a rapid shift in the graphite temperature. Thus, rapid feedback is dominated by fuel temperature changes.

This study of the dynamic behavior of MSRE falls under two sub-categories. One deals with the behavior of the reactor during normal operation when subjected to relatively small reactivity perturbations. The main concern here is to analyze the stability of the reactor under all power levels and compare results of simulations with experimental data. The other sub-category considers the response of the reactor system to significant and rapid changes in reactivity encountered during operational anomalies such as failure of either salt pumps or overcooling of the salts.

When operating at zero power or at a very low power, MSRE tends to be sluggish. At these power levels, the fission chain reaction is controlled using control rods alone, and the dynamic behavior depends on the prompt neutron lifetime and the effective delayed-neutron fraction. While operating at high power, the kinetic behavior of MSRE is dependent on the fuel and graphite temperature coefficients of reactivity, the power density of the

fuel, heat capacities of the various components, heat transfer coefficients, and transport lags in the salt circuits (Kerlin et al., 1971; Haubenreich et al., 1964).

The MSRE system has an overall negative reactivity coefficient. The dominant effect here is the change in the fuel salt density upon temperature increase that reduces the amount of fissile material present in the core leading to more neutron leakage. The graphite also has a negative feedback coefficient, due to a combination of leakage and spectral effects.

3. Development of the nodal model

The objective in this section is to develop nonlinear models that succinctly describe the MSRE system. A general description of these models is provided in Section 3.1. Modifications made to the one-region model for simulating operational anomalies are discussed in Section 3.2. This is followed by a brief discussion of the parameters of modeling along with the task of assembling them by combing literature resources in Section 3.3. The equations used in modeling are outlined with a brief discussion of the rationale behind using them in Section 3.4.

As mentioned before, the modeling approach is an extension of the approach detailed in Singh et al. (2017a). The importance weighting for each of the regions is adapted from the final ORNL model published in Kerlin et al. (1971b), and elaborated originally for a 10 MW(th) U-235 fueled MSRE system in Ball and Kerlin (1965). The aim of this paper is to validate the modeling approach by comparing results of simulations from both the models with experimental data from MSRE, published in Kerlin et al. (1971a)).

3.1. Description of the model

The essence of the modeling approach is to describe the dynamics of neutron density (reactor power), core heat transfer, heat exchanger, and radiator using nodalization of the various masses involved. This distributed-parameter modeling approach is similar to the one employed in Kerlin et al. (1971a), but using nonlinear neutron kinetics thanks to advances in computing power. Initially, a simple model with this approach was developed for the two-fluid MSBR researched during MSRP. A more detailed model of the core and associated feedback was drawn up in Singh et al. (2017a). The models presented here extend the same approach to the MSRE system.

A modified point kinetics model with six delayed-neutron groups is the basis for the described neutron dynamics for both models, and both U-233 and U-235 fuel. This neutron dynamics model explicitly accounts for delayed-neutron losses in the external loop through the heat exchanger. Expressing the neutronic equations in the form of fractional power excludes the need for quantitative knowledge of the neutron density and precursor concentrations. The premise is that the reactor power is proportional to neutron density, with all other parameters held fixed. The nine-region model accounts for spatial variation in power production and feedback effects by using importance weighting. The masses of the nine regions along with residence times and power generation fractions are adapted from Ball and Kerlin (1965). No spatial variations of neutron flux are considered in the one-region model.

Fig. 2 shows the one-region model for the MSRE.[2] Except for the core, the flow described in Fig. 2 applies to both the designed models. The core heat transfer description for the one-region model consists of one graphite node and two fuel flow nodes. For the nine-region model, the core is divided radially from the center into nine regions for a total of nine graphite nodes and eighteen fuel flow nodes. The nodalization for the nine-region model is shown in Fig. 3, which essentially reproduces the model developed by ORNL.[3]

Ordinary differential equations describe all corresponding state variables with delay terms included as required. Of the total power generated by fission, 93% is deposited in the fuel salt itself, while 7% goes to graphite in both models. For the nine-region model, the deposited power is distributed among the twenty-seven nodes as governed by axial and radial importance profiles for the fuel and graphite. These are just a proxy for the overall energy distribution and neutron flux profile in the core found by solving steady-state two-group diffusion equations in two dimensions as reported in Ball and Kerlin (1965). The weighted values of nuclear importance for each of the regions is used to calculate the temperature feedback reactivity from that region. Additionally, the liquid salt nodes are assumed to be well-mixed in both models with the temperature of the liquid exiting the node being the same as the temperature of the liquid in the node. Note that there is no radial or axial heat transfer in the graphite in both models. The one-region model therefore ignores the temperature distribution in the core. For the nine-region model, the core is divided radially into four flow columns each with a different mass flow rate such that the average residence time of the fuel salt in the core is the same as in the case of the one-region model. The most significant difference between the one-region model and the nine-region model is the effect of the higher core resolution on the average temperature and the resulting reactivity feedback. Following a reactivity perturbation in steady-state, the temperature response of downstream fuel flow nodes is affected by both the power generation in the node and temperature change in upstream nodes. The effects of this on the reactor response will be analyzed later.

Since the fractional power generated in the four radial columns are different, the salts exiting at the top have different temperatures. A 2-s mixing pot is used to facilitate mixing before the fuel salt moves on to the heat exchanger. The transit of the fuel salt to and from the heat exchanger is modeled using pure delays. The secondary salt circuit also utilizes appropriate delays. The fuel salt heat exchanger is modeled using four fuel flow nodes, four coolant flow nodes and two tube metal nodes. The heat sink in the one-region model is a radiator model consisting of one coolant salt node and one air flow node. This also allows for simulating pump trips in both the primary and secondary circuits. The nine-region model approximates the secondary side dynamics with a constant power withdrawal node representative of a radiator.

These models are intended to be a close approximation of the operational MSRE. Their inherent nonlinearity makes the predicted response more valid in scenarios away from the steady-state or what would serve as a point of linearization. Coupled with their simplicity of implementation, these models can be used to study the behavior of the reactor due to reactivity perturbations during normal operation. They can also be extended to study operational anomalies that lead to large reactivity excursions, as will be demonstrated. However, the models do have certain limitations. First, the neutronics and the precursors in the core are modeled as a point neglecting any effects of precursor drift within the core volume. Then there are reactivity effects due to xenon poisoning and circulating void fractions in the fuel salts that are ignored. The heat produced in the salt due to fissions out of the core and any decay of fission products are also neglected. Thus, these models serve as a faithful approximation of the MSRE system, barring the limitations mentioned above. If the modeling results compare favorably against experimental data, this modeling approach can

[2] https://github.com/ondrejch/2017-MSRE-paper/one-region_model.

[3] https://github.com/ondrejch/2017-MSRE-paper/nine-region_model.

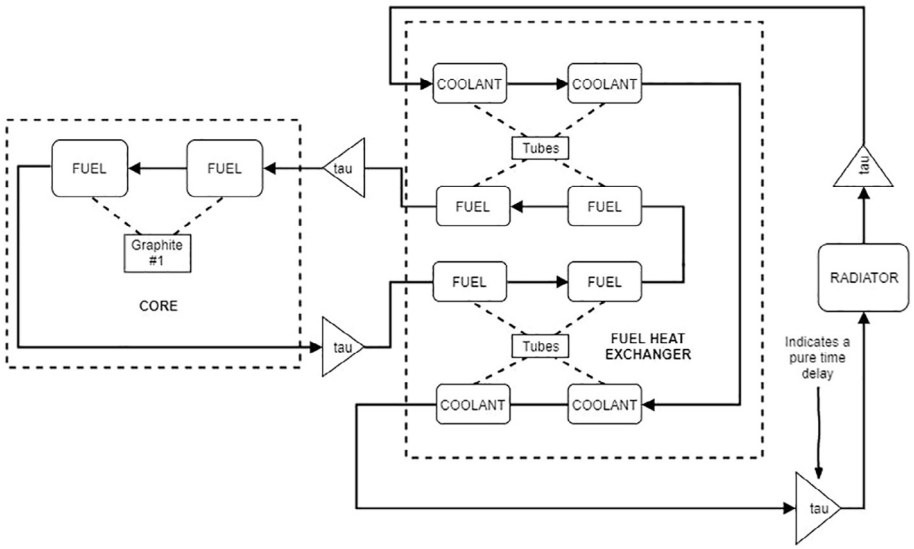

Fig. 2. MSRE one-region nodal model.

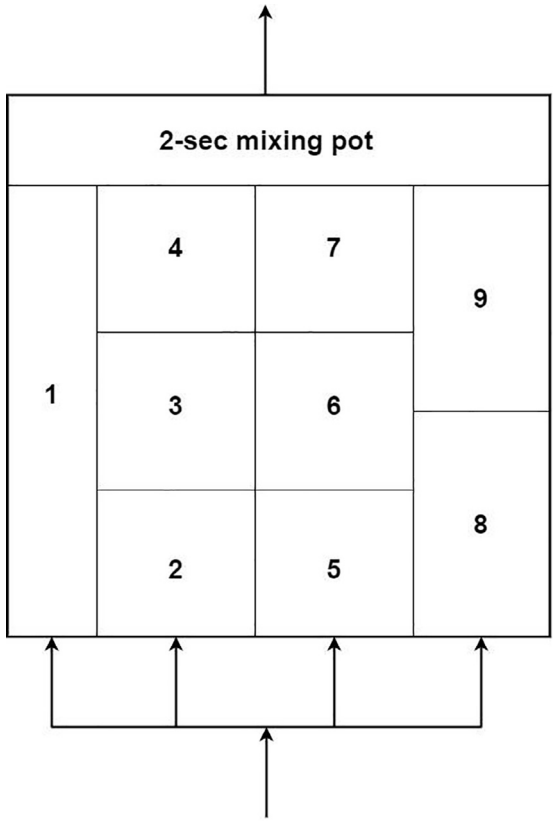

Fig. 3. Nine-region core as described in the model outlined in Kerlin et al. (1971a), (Source: ORNL, Ref. Kerlin et al. (1971)).

be extended to study the dynamic behavior of other MSR systems given a set of design parameters.

This model does not include any control action and when running at a constant flow rate can be considered valid for high power operation only, that is, 1 MW(th) and up. The model was developed in MATLAB™–Simulink, using appropriate tools for graphically representing the nodal model and solving the coupled nonlinear system of equations (Klee and Allen, 2011). Fig. 4 shows the block diagram of the model as assembled in Simulink. Implementing the neutronics required solving delayed-differential equations (DDE) for the delayed-neutron precursor concentrations. It should be mentioned that Simulink does not offer solvers for DDEs and hence delay terms for DDEs implemented in this model are stored and passed to an ODE solver after appropriate time delays.

3.2. Modifications for simulating operational anomalies

The operational anomalies discussed in this paper include loss-of-flow incidents at high power in the primary and the secondary system, and an uncontrolled "cold-slug" insertion into the core.[4] In the case of loss-of-flow in either circuit, the two major changes from the above-discussed model are in the transport lags used for simulating fluid flow in the system and the heat transfer coefficients for the various heat transfer interfaces.

During critical operation, a pump trip in the primary circuit affects the fuel circulation rate and hence the rate at which delayed-neutron precursors are transported. After the pump trip, the flow rate does not immediately fall to zero. Instead, there is a coast-down over a period of several seconds. This change in flow rate is simulated using an exponential decay function with appropriate time constants. The delays in the circuit are calculated as a function of the instantaneous flow rate over the coast-down period. Furthermore, the flow rate never reaches zero as there is some flow remaining due to thermal convection ensuing from temperature differences across the closed loop. These effects combined introduce power and temperature excursions resulting from both a reduction in the heat removal and an increased decay of delayed-neutron precursors in the core.

A similar implementation is used to simulate loss-of-flow in the secondary coolant loop. In this case, the delays in the secondary circuit are altered as per the instantaneous flow rate during the coast-down period. The instantaneous flow fraction is calculated during the coast-down by the "pump trip" subsystem (shown in Fig. 3) and passed on to the other plant subsystems. The heat transfer coefficients for the salt-graphite and salt-metal interfaces as a function of flow rate were obtained from studies conducted at ORNL for the MSRE system such as MacPherson (1960) and Burke (1960). These values are implemented as fractions of the nominal value in both cases.

[4] https://github.com/ondrejch/2017-MSRE-paper/operational_anomalies.

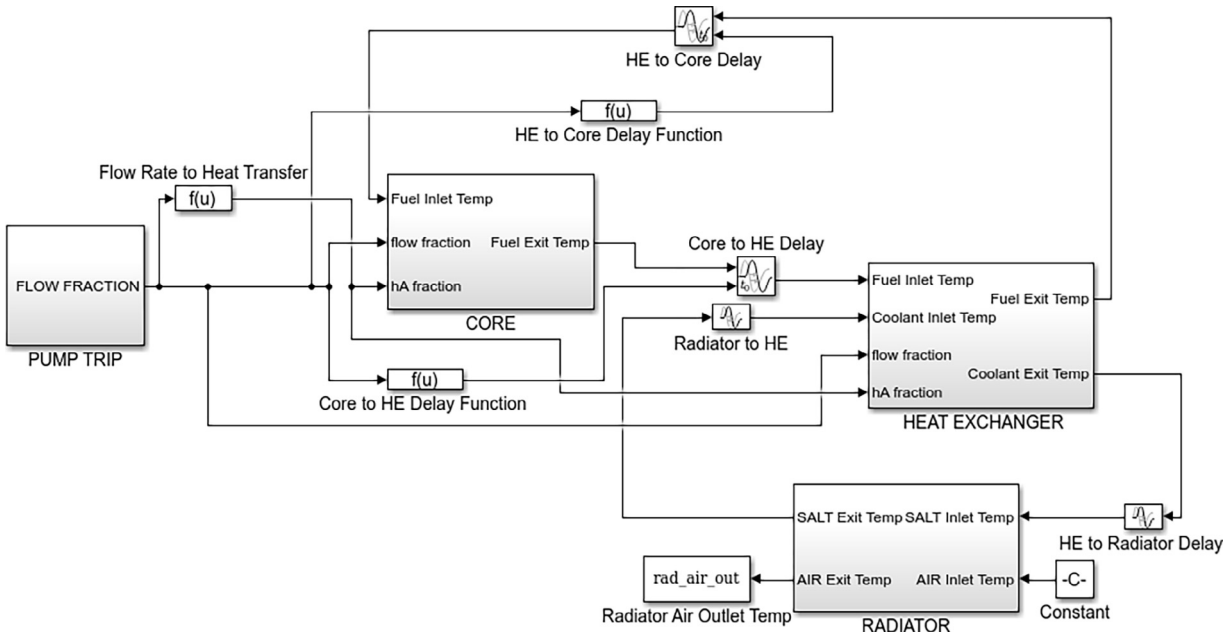

Fig. 4. Block diagram of the model assembled in Simulink.

A "cold-slug" incident refers to a decrease in the mean temperature of the core brought about from the injection of a small mass of fuel salt at an abnormally low temperature. The effect is an increase in reactivity because the fuel salt has a negative temperature coefficient. A cold-slug is simulated using a switch in the model that when tripped causes the inlet fuel temperature to decrease for a given period. Depending on the time the switch is activated, a certain volume of colder fuel salt flows into the core.

It must be mentioned that no corrective action is performed for the anomalies described above. Moreover, no phase change due to a freezing of the salts is accounted for in the present model. The MSRE system included heaters to prevent salts from freezing in the circuits, which are ignored in this model.

3.3. Parameters used in modeling

It is important to recognize that ORNL conducted the MSRE project over the course of a decade. A significant effort was devoted to archiving the knowledge attained during their program. An expansive library of documents and reports related to various aspects of the study were published over the entire period of the experiment.

Being an active research project meant that small changes in the reactor's design were frequent in the early stages. Moreover, MSRE was originally intended to be a 10 MW(th) reactor but ended up close to ~8 MW(th) as mentioned above. The various reports published before the full power operation detailed the version of the reactor as envisioned during the publication. This presents a challenge in gathering a consistent set of parameters that were representative of the final reactor operation. Thus, a significant undertaking in this project included gathering a parameter set that represents the version of the reactor where the experimental data were collected. It was determined that a preliminary set of parameters should be acquired from published design reports prior to full power operation, i.e., Haubenreich et al. (1964), (Robertson (1965) and Ball and Kerlin (1965). Any published parameters found in later reports that were different from those presented in the preliminary set took precedence, that is Steffy (1970) and Kerlin et al. (1971b).

Neutronics parameters used for the respective fuel types are presented in Table 1. Delayed-neutron data for the two fuel types is given in Table 2. The columns titled U-233 and U-235 correspond to values for the enrichments mentioned above. A concise set of physical modeling parameters is presented in Table A1. The nuclear importance weighted parameters used in the nine-region model is reproduced from Ball and Kerlin (1965), in Table A2. A digital version of the entire set of parameters will be made available online with the publication of this paper.

3.4. Equations used in modeling

The neutron dynamics is described by the modified Point-reactor Kinetics Equations (PKE), similar to those employed in earlier studies of MSRE (Kerlin et al., 1971). The main difference here

Table 1
Neutronics parameters for U-233 and U-235 (Kerlin et al., 1971; Ball and Kerlin, 1965).

Parameter	U-235	U-233
Prompt neutron lifetime Λ	4×10^{-4} s	2.4×10^{-4} s
Delayed-neutron fraction β	0.0065	0.00264
Core transit time τ_C	8.46 s	8.46 s
External loop transit time τ_L	16.73 s	16.73 s
Fuel salt reactivity coefficient α_f	-8.71×10^{-5} δρ/°C	-11.034×10^{-5} δρ/°C
Graphite reactivity coefficient α_g	-6.66×10^{-5} δρ/°C	-5.814×10^{-5} δρ/°C

Table 2
Delayed-neutron group data for U-233 and U-235 (Steffy and Wood, 1969).

	U-233		U-235	
Group	λ_i (sec^{-1})	β_i (x 10^{-4})	λ_i (sec^{-1})	β_i (x 10^{-4})
1	0.0126	2.28	0.0124	2.23
2	0.0337	7.88	0.0305	14.57
3	0.139	6.64	0.111	13.07
4	0.325	7.36	0.301	26.28
5	1.13	1.36	1.14	7.66
6	2.50	0.88	3.01	2.80
Total		**26.40**		**66.61**

is that the model is inherently nonlinear. Shown here in Eqs. (1) and (2), these are a system of seven, coupled, nonlinear, delayed-differential equations.

$$\frac{dn(t)}{dt} = \frac{(\rho(t)-\beta)}{\Lambda} n(t) + \sum_{i=1}^{6} \lambda_i C_i(t) + S(t) \tag{1}$$

$$\frac{dC_i(t)}{dt} = \frac{\beta_i}{\Lambda} n(t) - \lambda_i C_i(t) - \frac{C_i(t)}{\tau_C} + \frac{C_i(t-\tau_L) e^{-\lambda_i \tau_L}}{\tau_C} \tag{2}$$

where **n(t)** is neutron density, $\mathbf{C_i(t)}$ represents the concentration of the i^{th} delayed-neutron precursor (where, i = 1…6), **ρ(t)** is the total reactivity as a function of time (input), $\boldsymbol{\beta_i}$ is the delayed-neutron fraction of the i^{th} delayed group, **β** is the total delayed-neutron fraction, **S(t)** is the source perturbation term, $\boldsymbol{\tau_C}$ is the fuel transit time in the core (8.46 s), and $\boldsymbol{\tau_L}$ is the fuel transit time in the external loop (16.73 s).

With the above modifications, the reactivity necessary for steady state operation $\boldsymbol{\rho_o}$ is non-zero, unlike in the case of solid-fuel reactors. It is obtained by setting the derivatives on the left side of Eqs. (1) and (2) equal to zero and solving for **ρ(t = 0)**. It is given by:

$$\rho_o = \beta - \sum_{i=1}^{6} \frac{\beta_i}{\left(1 + \frac{1}{\lambda_i \tau_C}[1 - e^{-\lambda_i \tau_L}]\right)} \tag{3}$$

This $\boldsymbol{\rho_o}$ term is the reactivity change due to circulating fuel and accounts for delayed-neutrons lost in transit. It is dependent on the fissile material and has a value of $\boldsymbol{\rho_o} \approx 0.00247$ for U-235 fuel, and $\boldsymbol{\rho_o} \approx 0.00112$ for U-233 fuel. When the reactor model operates at steady-state, the natural reactivity feedbacks from the fuel and graphite sum up to this value. Thus, $\boldsymbol{\rho_o}$ can be viewed as the reactivity needed to achieve steady state in going from a stationary solid fuel to a circulating fluid fuel.

The total reactivity for the system is expressed as:

$$\rho(t) = \rho_o + \rho_{fb}(t) + \rho_{ext}(t) \tag{4}$$

The feedback reactivity, $\boldsymbol{\rho_{fb}(t)}$, is contributed by changes in the fuel salt, and graphite temperatures. It is given by,

$$\rho_{fb}(t) = \alpha_f \sum_{i=1}^{n} I_{fi}\left[T_{f,0} - T_f(t)\right] + \alpha_g \sum_{i=1}^{n} I_{gi}\left[T_{g,0} - T_g(t)\right] \sum_{regions} I_{fi} = 1.0, and \sum_{regions} I_{gi} = 1.0 \tag{5}$$

where the terms represent a contribution from fuel and graphite given by the product of the reactivity feedback coefficient ($\boldsymbol{\alpha_f}$, $\boldsymbol{\alpha_g}$), the weighted nuclear importance factor and the difference of the temperature of each node at time 't' from the steady-state temperature of that node. Also, the sum of the importance factors for each component is unity. The sign of each term depends on the temperature variations in the node and therefore when summed together, $\boldsymbol{\rho_{fb}}$ can have a net positive or negative value.

The total heat from fission is deposited in the core components in the fractions mentioned before, and all this heat is carried away by the fuel salt which is the primary coolant. Thus, the temperature change equation for the fuel salt contains a fractional power generation term, a fuel to fuel node heat transfer term, and a fuel to graphite heat transfer term, as shown in Eqs. (6) and (7). Additionally, this means that steady-state temperature of the graphite node is higher than the fuel nodes because all the heat generated in the graphite eventually needs to be carried away by the fuel salt.

$$\frac{dT_{f1}}{dt} = \frac{W_f}{m_{f1}}\left(T_{f_{in}} - T_{f1}\right) + \frac{K_1 P_0 \left(\frac{n}{n_0}\right)}{m_{f1} C_{pf}} + \left(\frac{K_{g1}}{K_{g1}+K_{g2}}\right) \frac{hA_{fg}}{m_{f1} C_{pf}} \left(T_g - T_{f1}\right) \tag{6}$$

$$\frac{dT_{f2}}{dt} = \frac{W_f}{m_{f2}}\left(T_{f1} - T_{f2}\right) + \frac{K_2 P_0 \left(\frac{n}{n_0}\right)}{m_{f2} C_{pf}} + \left(\frac{K_{g2}}{K_{g1}+K_{g2}}\right) \frac{hA_{fg}}{m_{f2} C_{pf}} \left(T_g - T_{f1}\right) \tag{7}$$

Here, $\mathbf{W_f}$ is the mass flow rate of fuel salt, $\mathbf{m_{f1}}$ and $\mathbf{m_{f2}}$ represent the mass of fuel nodes '1' and '2' respectively, $\mathbf{C_{pf}}$ represents the fuel salt specific heat capacity, $\mathbf{K_1}$ and $\mathbf{K_2}$ are the fraction of total power generated in fuel nodes '1' and '2', $\mathbf{K_{g1}}$ and $\mathbf{K_{g2}}$ represent the fraction of power generated in the graphite transferred to each fuel node, $\mathbf{hA_{fg}}$ is the product of area and heat transfer coefficient for the fuel-graphite interface, $\mathbf{P_o}$ is the nominal power which multiplied with fractional neutron density $\mathbf{n/n_o}$ gives the instantaneous power, and the **T**s represent the temperatures of the various nodes. Note that the direction of heat transfer depends on the instantaneous temperature of the various nodes.

The graphite node contains a power generation term, since 7% of the power is deposited in the graphite, and a fuel to graphite heat transfer term, as in Eq. (8).

$$\frac{dT_g}{dt} = \left(K_{g1} + K_{g2}\right) \frac{P_0 \left(\frac{n}{n_0}\right)}{m_g C_{pg}} + \frac{hA_{fg}}{m_g C_{pg}} \left(T_f - T_g\right) \tag{8}$$

Here, $\mathbf{m_g}$ represents the mass of the graphite node, $\mathbf{K_g}$ is the fraction of heat deposited in the graphite node, and $\mathbf{C_{pg}}$ is the graphite specific heat capacity. All other terms have the same meaning as before. Similar equations are constructed for each region in the nine-region model.

Heat exchanger and radiator nodes use analogous equations as described above, but without the power generation terms as no heat generation outside the core is considered in this model. Steady-state temperatures throughout the model were adopted from MSRE design documents. In the one-region model, the mass of the various components is distributed equally among the nodes, and intermediate nodal temperatures are calculated by dividing the difference in the inlet and outlet temperatures equally. For the nine-region model the steady-state temperature in each region is determined using nuclear importance factors detailed in Table A2.

In the case of loss-of-flow simulations, the instantaneous flow rate is used to recalculate time delays between the reactor core and heat exchanger, the total time spent in the core, and the time spent traveling through the primary circuit. The change in delays causes the neutronics equations to change as well. The new neutronics equations are given in Eqs. (9) and (10). The precursor concentrations are modified to account for the changing rate of precursors leaving and reentering the core. Thus, the delay terms $\boldsymbol{\tau_C}$ and $\boldsymbol{\tau_L}$ for the pump trip scenario are not constants anymore but rather functions of time. Eq. (9) represents the precursors leaving the core at time 't', which can in turn, be substituted into Eq. (2) to produce Eq. (10).

$$\psi_i(t) = \frac{C_i(t)}{\tau_C(t)} \tag{9}$$

$$\frac{dC_i(t)}{dt} = \frac{\beta_i}{\Lambda} n(t) - \lambda_i C_i(t) - \psi(t) + \psi_i(t - \tau_L(t)) e^{-\lambda_i \tau_L(t)} \tag{10}$$

4. Results

The results from simulation and comparison with experimental data, when available, are presented in this section. The experimental data were retrieved from Kerlin et al. (1971a) and Steffy (1970), by digitizing the plots (Rohatgi).[5] Results for the U-235 fueled sys-

[5] https://github.com/ondrejch/2017-MSRE-paper/MSRE_data.

tem are presented in Section 4.1, followed by results from the U-233 system in Section 4.2. Finally, results from simulation of operational anomalies are presented in Section 4.3.

4.1. U-235 fueled system

This section deals with model simulations using neutronics parameters for U-235 fuel. Thermodynamic parameters are assumed to be the same for both fuel types.

4.1.1. Dynamic response to a step reactivity insertion

The dynamic characteristics of the MSRE models are studied by examining the response to a step reactivity change. The response of both the models for the U-235 fueled MSRE system using a +10 pcm reactivity input is shown in Fig. 5 for thermal power levels of 1, 5, and 8 MW(th). At low power levels, such as 1 MW and below, the MSRE system tends to be sluggish, as expected (Ball and Kerlin, 1965). The temperature differences in the core components, primarily the fuel salt, is not sufficient to generate a strong feedback response. Therefore, the power response following a step perturbation is lightly damped and the system tends to be oscillatory with a low frequency. As power level increases, the increasing feedback reactivity counteracts the external reactivity perturbation and strongly damps the response. The peaks in the response of the two models, at all power levels investigated, varied in that the nine-region model always showed a lower magnitude. The nine-region model also showed a phase difference. The conservative response of the one-region model for the initial power spike due to model limitations within the core residence time. The nine-region model resolves the temperature distribution and the relevant feedbacks within the core and hence shows a more detailed response. The long-term behavior, however, is similar for both the models. The response was also progressively more damped at higher power levels for both models.

The transient response at nominal power of 8 MW(th) to a +50 pcm step insertion is shown in Fig. 6, along with the corresponding feedback reactivity response resulting from the associated temperature changes in the core. A prompt jump in power is seen immediately following the step insertion with a peak around ~17 s followed by an exponential decrease. A corresponding "plateau" is seen in the feedback response at ~17 s. Because of the circulating fuel, warmer fuel salts from the initial transient reenter the core every ~17 s. This is, of course, the external loop time of the fuel. For circulating fuel reactors, the steady-state reactivity is non-zero, as mentioned before. This means that the reactivity feedback changes about a steady-state value of ρ_o. The feedback plot shows a corresponding prompt decrease in the reactivity immediately following the step insertion. As the fuel and the graphite temperatures increase, the feedback reactivity settles at a value lower than steady-state counteracting the step insertion. The average temperatures of the graphite and core fuel flow nodes for both models are shown in Fig. 7. Following the step insertion, the fuel temperatures increase sharply in both models. It is evident that

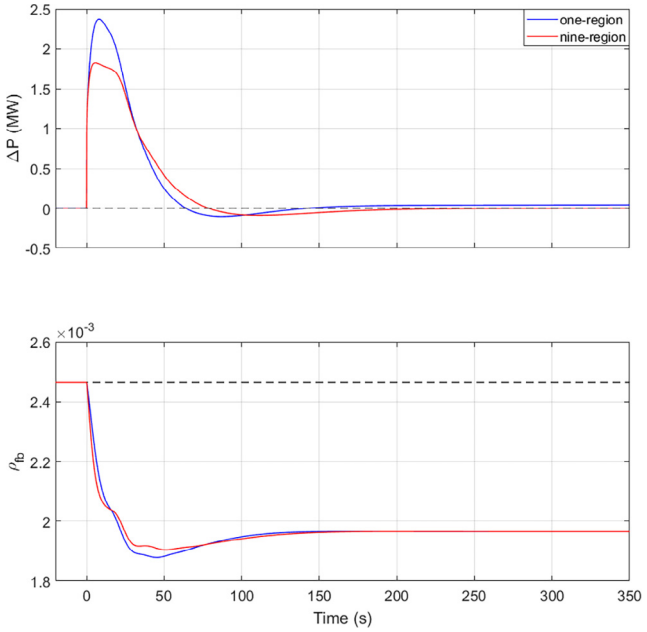

Fig. 6. Response of the reactor power operating at 8MW(th) to a +50 pcm step insertion (top) power over time (bottom) corresponding feedback reactivity over time.

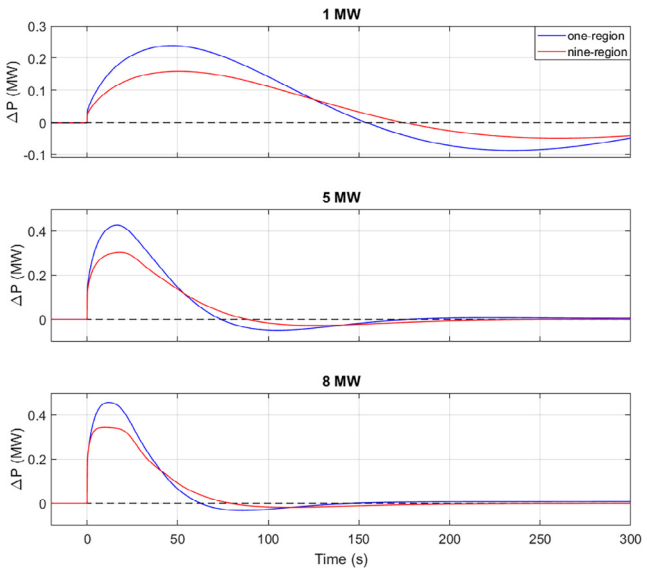

Fig. 5. Response of power over time for the U-235 fueled MSRE system to a +10 pcm reactivity input at 1, 5, and 8 MW(th).

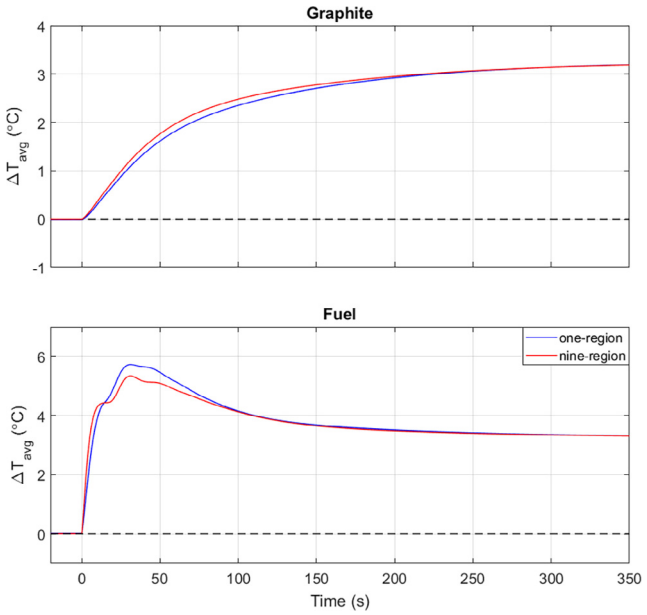

Fig. 7. Graphite and fuel node temperatures in the core following +50 pcm external step reactivity insertion.

the increased nodalization along with distinct flow rates in the flow columns of the nine-region model leads to a higher resolution in the fuel temperature response. The graphite temperatures are seen to increase smoothly to an increased steady-state value in each model. Because of the increased average nodal temperatures, a corresponding feedback response of -50 pcm is generated counteracting the step perturbation.

4.1.2. Power to reactivity frequency response

In this case, published experimental data was available and digitized as mentioned before. For this type of modeling, the usual route is to linearize the model and calculate frequency response using well-established methods for linear time invariant systems. The models covered in this paper, however, are nonlinear. Therefore, a sinusoidal reactivity input of small amplitude of ±1 pcm was used to produce the Bode plots. For such small perturbation, both models responded well within the domain of linearity. That is, the frequency of the power response was the same as the frequency of the periodic reactivity input. The changes in the gain and phase of the power response were calculated using appropriate algorithms.

Fig. 8 shows a comparison of the power to reactivity frequency response for the MSRE system using U-235 fuel at 5 MW(th) compared to the experimental data given in Kerlin and Ball (1966). Fig. 9 shows the same at 8 MW(th). The magnitude plots display a prominent peak with the magnitude indicative of the natural period of the system. The peak shifts to lower frequencies at lower power levels as seen in the figures. A dip in the magnitude at ~0.25 rad/s, however, is seen at all power levels for both core models. This can be attributed to the recirculation of the fuel. Consider a small mass of fuel salt entering at the bottom of the core. After undergoing fission, this mass of fuel salt with its load of delayed neutron precursors reenters the core after one full loop. Thus, new delayed neutron precursors are reintroduced into the core every $\tau_L + \tau_C$ seconds where they decay affecting power and feedback response. Thus, the reactor has a natural resonance response at a frequency of $2\pi/(\tau_L + \tau_C) \approx$ **0.25 rad/s**.

As expected from the time response plots shown above, the magnitude of the nine-region is typically lower than the one-region model. There is also a slight difference in the phase. The response of the nine-region model developed here is identical to the model published by Kerlin et al. (1971b). Results for both models show good general agreement with the experimental data. Note that some errors may have been introduced during the digitizing process owing to the fact that the data were originally reported on hand-drawn plots, then scanned and made available. Barring such sources of error, the differences between simulation and experimental data can be attributed to the inherent simplifications in the model and any differences in parameters. The general accuracy of the models shows that the difference in core nodalization has a minimal effect on the response of the dynamic model. Each model is a good approximation of the MSRE system and the responses generated are essentially valid when compared to experimental data. Notably, it appears that the simplest one-region, one-dimensional model is sufficient to reproduce the available experimental data.

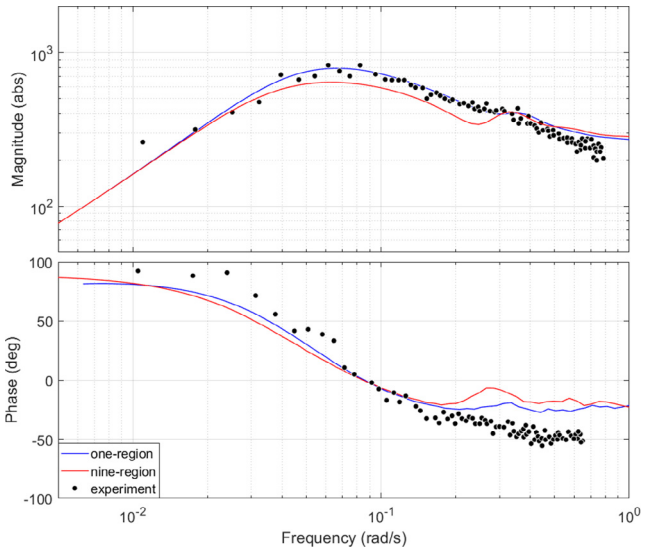

Fig. 9. Comparison of power to reactivity frequency response of the model to experimental data for U-235 fuel at 8 MW(th), (a) magnitude and (b) phase.

4.2. U-233 fueled system

Modeling results with U-233 fuel are presented here along with comparisons with experimental data obtained from MSRE reports.

4.2.1. Dynamic response to a step reactivity insertion

Fig. 10 shows the response of the U-233 fueled MSRE models to a step input of +10 pcm. Both models display stable behavior, comparable to the U-235 fueled case, despite the fuel now having a much lower delayed-neutron fraction. At lower power levels, the system tends to be sluggish and oscillatory, as with the U-235 case, but with a shorter period of oscillation. This can be attributed to the fact that U-233 fuel has a much stronger negative feedback coefficient. At higher power, the system response is strongly damped.

Notice that "plateaus" are seen in the transient response for the 5 and 8 MW cases. Due to the higher nodalization, the plateau is more noticeable in the nine-region model than in the one-region model. The explanation for this is as follows. The core power dramatically increases immediately following the step input accompanied by a rapid increase in the temperature of the fuel salt. After reaching a peak in the first couple of seconds, the negative feedback reactivity of the fuel stops any further increase in power. During this period "cold" salt from the heat exchanger at a con-

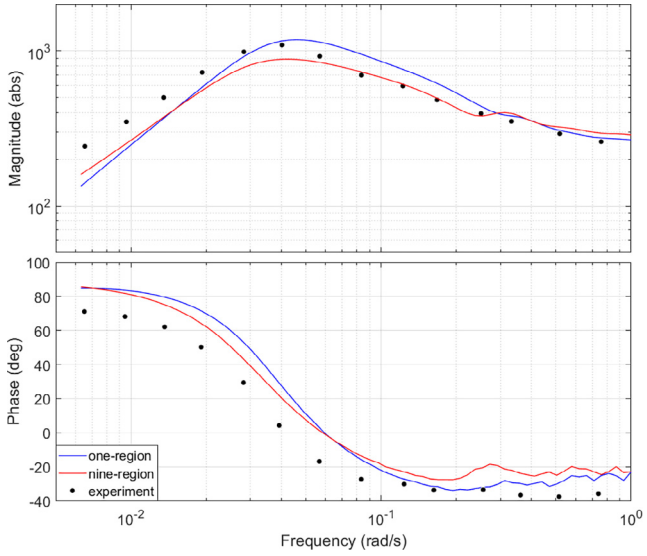

Fig. 8. Comparison of power to reactivity frequency response of the model to experimental data for U-235 fuel at 5 MW(th), (a) magnitude and (b) phase.

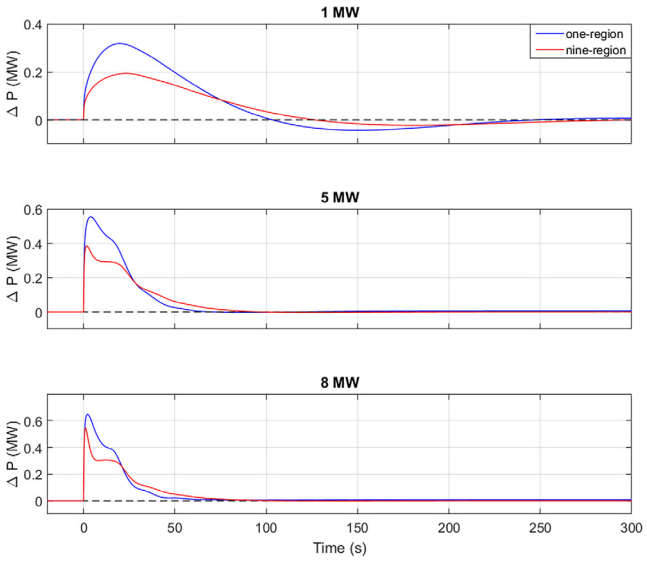

Fig. 10. Response of power over time for the U-233 fueled MSRE system to a +10 pcm step input at 1, 5 and 8 MW(th).

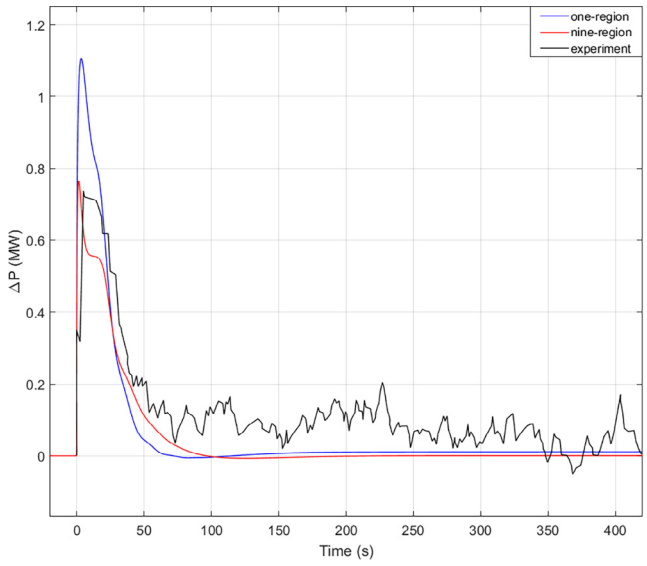

Fig. 11. Response of model compared with experimental data for a +19.6 pcm step insertion for the reactor at 5 MW.

stant temperature continues to flow into the core. The negative feedback of the salt at this time is sufficient to counteract the step input, and the power begins to level off briefly before "warmer" fuel salt from the initial reactivity insertion reenters the core after making a loop through the heat exchanger. This increase in average core temperature introduces further negative feedback again decreasing the power.

At lower power levels, the slower temperature increase in the fuel, and therefore the negative feedback, prevents the reactor power from reaching the peak of its first oscillation before "warmer" fluid returns to the core after making an external loop. Hence there is no plateau at 1 MW. Note also that this behavior is not seen in the U-235 case described earlier for the power levels investigated here. This is because of both a lower negative feedback coefficient of the U-235 fuel salt which does not damp power increase as strongly, and a higher delayed-neutron fraction that sustains the fission reaction longer leading to a smooth decrease in power. At higher power levels, U-235 fuel should also display analogous behavior.

Displaying the power response over time is more intuitive because human beings deal with time in day-to-day life. Hence, an effort was made to digitize the experimental data for step response of the MSRE system using U-233 fuel as published by Steffy (1970). The experimental data is noisy, but the power profile can still be deduced. This comparison for both the one-region and the nine-region models against experimental data is shown in Fig. 11, for the reactor at 5 MW. The step reactivity is +19.6 pcm. The one-region model has a higher peak compared to the nine-region model due to the reasons explained before. The response profile for both models, however, compare well with the experimental data. The response of the nine-region model is virtually identical to the theoretical ORNL model presented in Steffy (1970).

Before proceeding with this discussion, the reader is encouraged to compare the modeling results published here with Ball and Kerlin (1965) and Kerlin et al. (1971b). For a more modern take, the reader is directed to results of modeling efforts at Politecnico di Milano published by Guerrieri et al. (2011) and Cammi et al. (2012). The results for the nine-region model published here are essentially identical to the results published in Kerlin et al. (1971b), and the ORNL model as reproduced by Guerrieri et al.

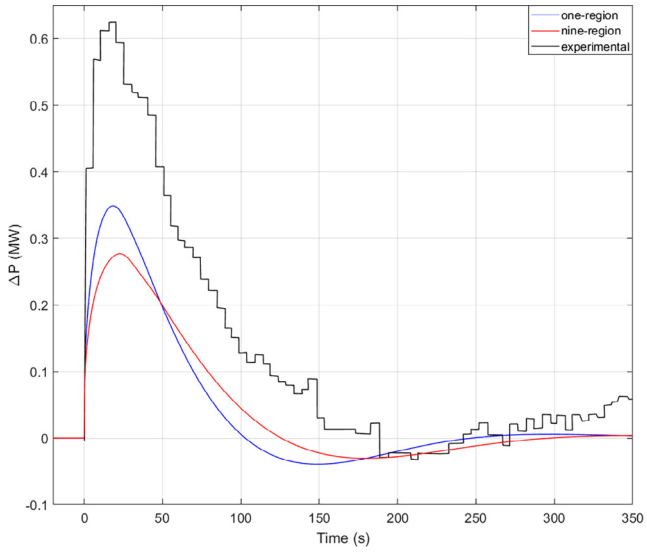

Fig. 12. Response of model compared with experimental data for a +13.9 pcm step insertion for the reactor at 1 MW.

(2011). With this in mind, a comparison of model results with experimental data with the reactor at 1 MW for a +13.9 pcm step insertion is presented in Fig. 12. A similar plot, for the reactor at 8 MW and a +24.8 pcm step insertion is shown in Fig. 13. In the 1 MW case, both the developed models clearly undershoot the experimental data. In the 8 MW case, the responses of models clearly overshoot the experimental data. The power response for the same input perturbations and power levels as Figs. 12 and 13 were published by Guerrieri et al. (2011), and their ORNL reproduction matches the nine-region model perfectly. Thus, we have two modern and independent modeling efforts that compare well with each other, but fail to agree with the experimental data. Furthermore, the theoretical model in the time response plots presented in Steffy (1970), matches the experimental data. This is a conundrum. On one hand, the frequency response plots for the nine-region model published here match the theoretical results

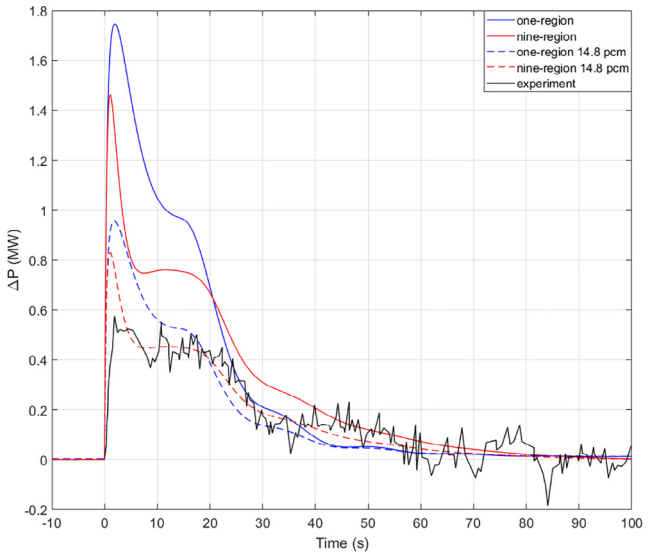

Fig. 13. Modeling results compared with experimental data for a +24.8 pcm step insertion for the reactor at 8MW. Response to a +14.8 pcm insertion is also shown.

published by Kerlin et al. (1971b), for all cases investigated. The comparisons also hold true with results published by Guerrieri et al. (2011). On the other hand, the time response plots match for the 5 MW case, but disagree for the 1 MW and 8 MW cases. Not to mention, the disagreements in model response and experimental data are inverted for the 1 MW and 8 MW cases. This may indicate an error in the data reported by Steffy (1970). While there can be many arguments made for this discrepancy, the authors would like to refrain from hypothesizing due to the absence of the original recorded data. Instead, a comparison of the models is presented for a step insertion of +14.8 pcm at 8 MW in Fig. 13. The models now compare favorably to the experimental data. Likewise, the results for the nine-region now matches the "theoretical model" in Steffy (1970). This is just conjecturing, but the intention is to point out that the results published for MSRE are not immune to errors. Additionally, this demonstrates limitations of existing

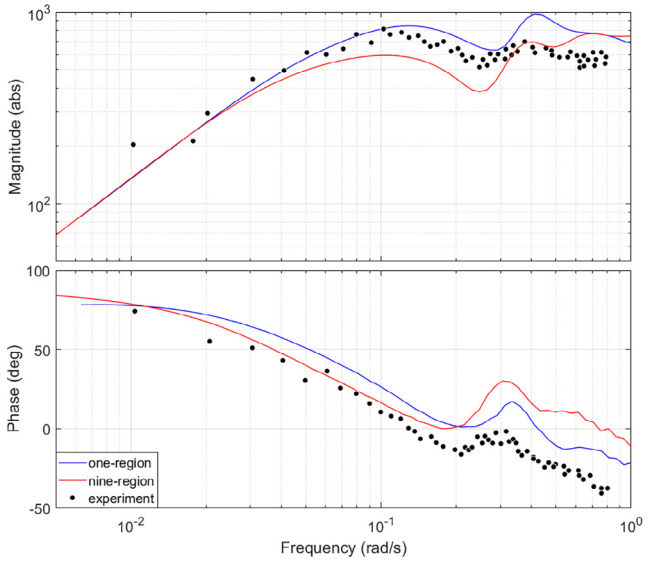

Fig. 14. Comparison of power to reactivity frequency response of the model with experimental data on U-233 fuel at 8 MW(th), (a) magnitude and (b) phase.

data (the MSRE results) to validate modern tools. Perhaps, a new molten salt reactor system built with the intention of benchmarking and code validation is needed.

4.2.2. Power to reactivity frequency response

The power to reactivity frequency response of the MSRE system at 8 MW(th) is shown in Fig. 14 plotted against experimental data from Kerlin et al. (1971a). The plot shows a general agreement of both the models with the experimental data. A dip in the magnitude at ~0.25 rad/s is seen, and as before, can be attributed to fuel recirculation effects.

4.3. Operational anomalies

Results from the simulation of credible operational anomalies using the developed one-region model are reported in this section. Loss-of-flow simulations were performed for both the primary (fuel) and secondary (coolant) salt loops. Simulations for a cold-slug of salt introduced into the core and the associated reactivity perturbation were also performed. In each case, the model operates at nominal power of 8 MW(th) and does not include corrective action or thermo-physics of phase changes in the salts.

4.3.1. Loss-of-flow in the primary system

The most likely cause of a loss-of-flow in the primary system is a pump trip, in which case the flow rate reduces exponentially over a coast-down period before reaching a steady-state thermal convection rate. The flow rate during coast-down is modeled using an exponential decay equation with time constants of 2 s, 6 s, and 10 s. The final thermal convection circulation rate is determined by temperature differences across the circuit which are not modeled here. Nevertheless, cases for different final circulation rates of 1%, 2%, 3%, 4%, and 5% of design flow rate are investigated here.

The heat transfer coefficient is dependent on the flow rate and decreases as the flow rate drops. As mentioned before, the heat transfer coefficient as a function of flow rate was obtained from MacPherson (1960), by digitizing the provided plot that has been reproduced here in Fig. 15(a) MacPherson (1960). This is used to adjust the heat transfer for the primary salt and graphite, and the primary salt and heat exchanger metal interfaces based on the instantaneous flow rate. Time delays in the primary circuit are also recalculated, as explained before.

The response of the core power following the pump trip is shown in Fig. 16 for the aforementioned time constants and a final thermal convection rate of 5% of nominal flow. The fissile fuel is U-235. Fig. 17 shows the average core fuel salt temperature for said coast-down rates. It is evident that the effect of different time constants on the rate of power change is negligible. The power in the core increases briefly following the pump trip due to more delayed-neutron precursors decaying in the core. It then falls sharply due to the strongly negative temperature feedback arising from the now warmer and slower moving fuel salt. Meanwhile, the average core fuel salt temperature first increases due to reduced heat transfer in both the core and the heat exchanger, and then decreases due to reduced fissions and continual heat removal by the secondary system. This lowered temperature coupled with the reintroduction of delayed-neutron precursors into the core after ~300s reignites the fission chain reaction. The power eventually settles at some rate lower than nominal power depending on the final convection flow rate and the temperature feedbacks. It should be mentioned that the temperature of both the fuel and coolant salts in the heat exchanger fall below their liquidus temperatures in the present model, since phase changes are not accounted for. The MSRE contained electrical heaters in all salt containing parts of the system to prevent unintended freezing

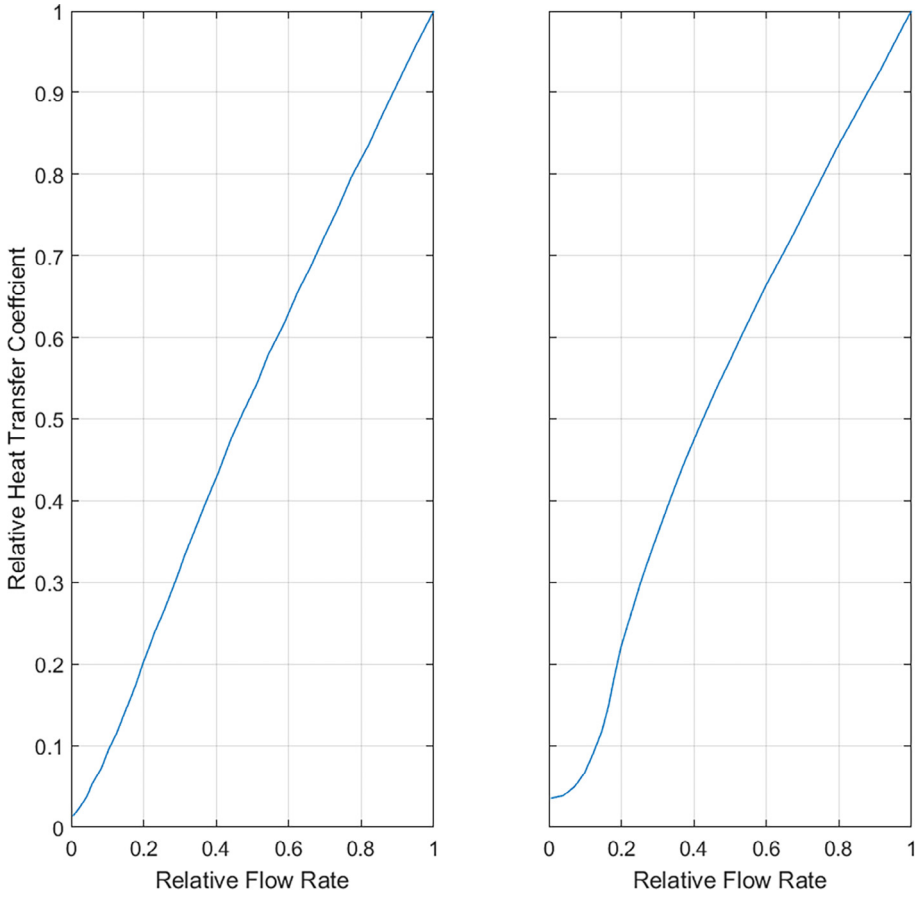

Fig. 15. Relative heat transfer coefficient versus relative flow rate for (left) primary loop (right) secondary loop.

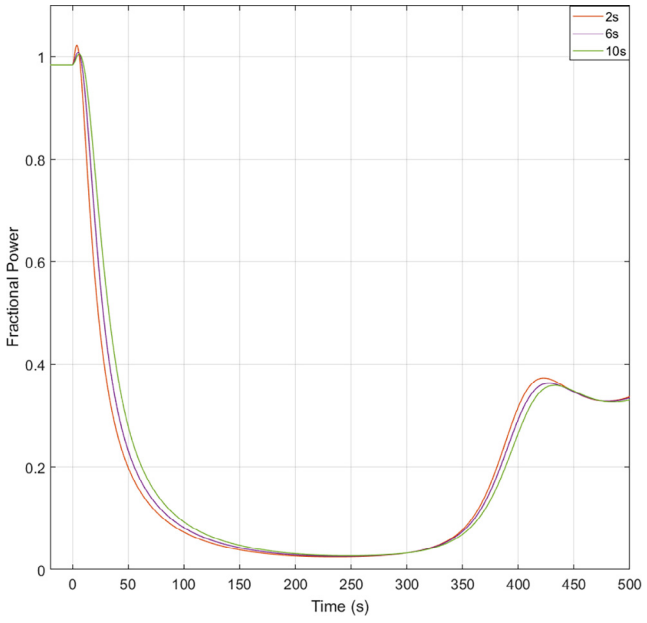

Fig. 16. Response of core power following pump trip in the primary circuit for different coast-down rates.

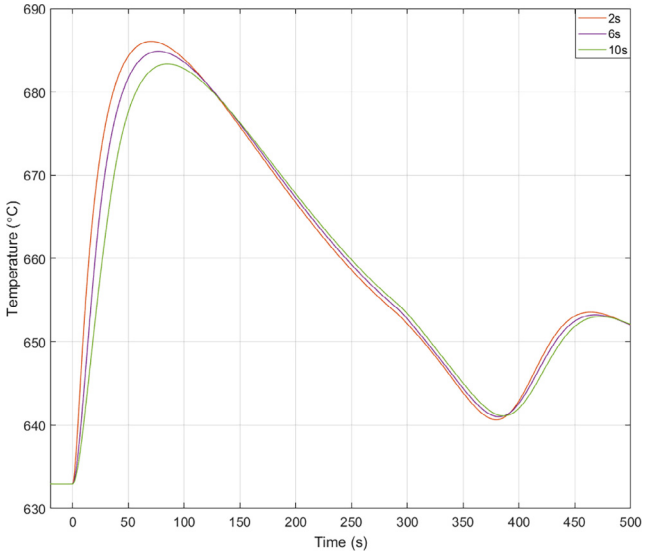

Fig. 17. Average core fuel salt temperatures following pump trip in the primary circuit for different coast-down rates.

and allow for salt draining at all times (Robertson, 1965). In addition to that, fission product decay heat that is not accounted here could prolong salt freezing. This means that in the actual MSRE system, the salt temperatures could have been higher, but the general behavior should remain the same. The model response here is comparable to the theoretical study published in Haubenreich and

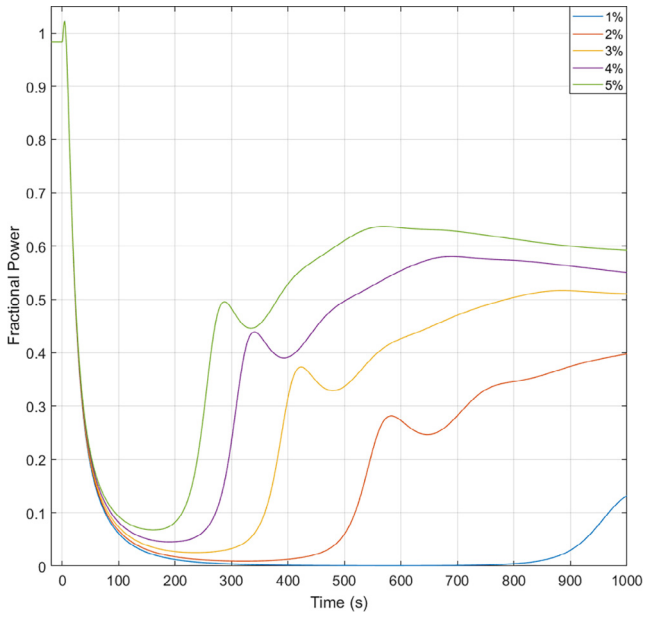

Fig. 18. Response of core power following pump trip in the primary circuit for different final steady-state thermal convection rates.

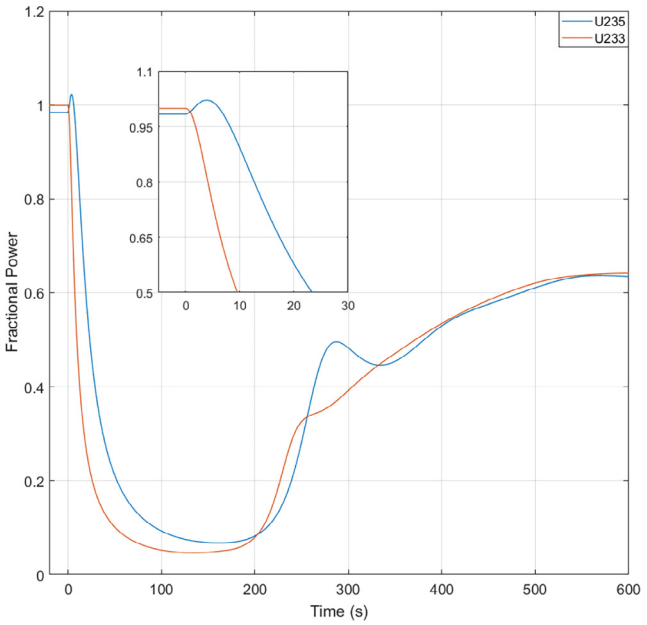

Fig. 20. Response of core power following pump trip in the primary circuit for U-235 and U-233 fuel. The first 30 s are shown in the insert.

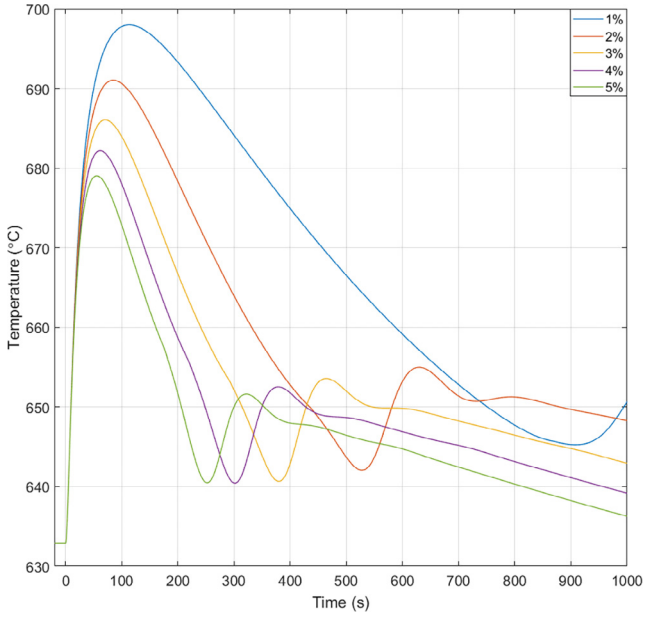

Fig. 19. Average core fuel salt temperatures following pump trip in the primary circuit for different final steady-state thermal convection rates.

Engel (1962). However, there is no experimental data for these anomalies from the MSRE.

Unlike the pump coast-down rate, however, the final steady-state thermal convection rate does indeed have an appreciable effect on the power response of the core. Following a pump trip, the power decreases because the fission rate is suppressed by the strong negative feedback until delayed-neutron precursors are reintroduced into the core. Consequently, a higher final flow rate would allow for more precursors to be reintroduced into the core and reignite the fission reaction. Furthermore, higher flow rates have higher heat transfer as evidenced by Fig. 17 leading to more cooling and a reduction in the average core temperature which weakens the negative feedback effect. The power response for the previously stated thermal convection flow rates for U-235 fuel are shown in Fig. 18. The accompanying average core fuel salt temperatures are presented in Fig. 19.

The effect of different fuel types in a pump trip scenario was also investigated. The power response following a pump trip with a coast-down time constant of 2 s and a final thermal convection rate of 5% for U-233 and U-235 fuel is shown in Fig. 20. The insert depicts the initial transient for the two fuel types immediately following the pump trip. The major differences here are that the initial increase in power is absent for U-233 fuel owing to its lower delayed-neutron fraction and higher negative feedback. Likewise, after the subsequent reintroduction of delayed-neutron precursors, the U-233 profile is strongly damped compared to U-235. In both cases, the power eventually levels out depending on the temperature feedback and the delayed-neutron fractions. Other aspects of the reactor showed no practical differences in behavior.

4.3.2. Loss-of-flow in the secondary system

A pump trip scenario can also arise in the coolant salt system. Loss-of-flow in this system is accompanied by a decrease in the heat transfer in the secondary system leading to less heat being withdrawn from the core and less heat deposited to the radiator. Fig. 15b) depicts the relation of heat transfer coefficient to relative flow rate obtained from Burke (1960).

The inlet and outlet temperature of the coolant salt in the heat exchanger is plotted in Fig. 21. The power response for different final thermal convection rates is shown in Fig. 22, and corresponding average core temperatures are plotted in Fig. 23. The coolant salt outlet temperature from the heat exchanger rises sharply following the pump trip. This leads to a sharp decrease in the power response driven by a rapid increase in average core fuel salt temperature and the resulting negative feedback. This feedback is sufficient to suppress the fission reaction, even more so than in the case of the primary pump trip, especially at lower final thermal convection rates in the secondary system. As a consequence of the reduced energy deposition from fission, the average core fuel

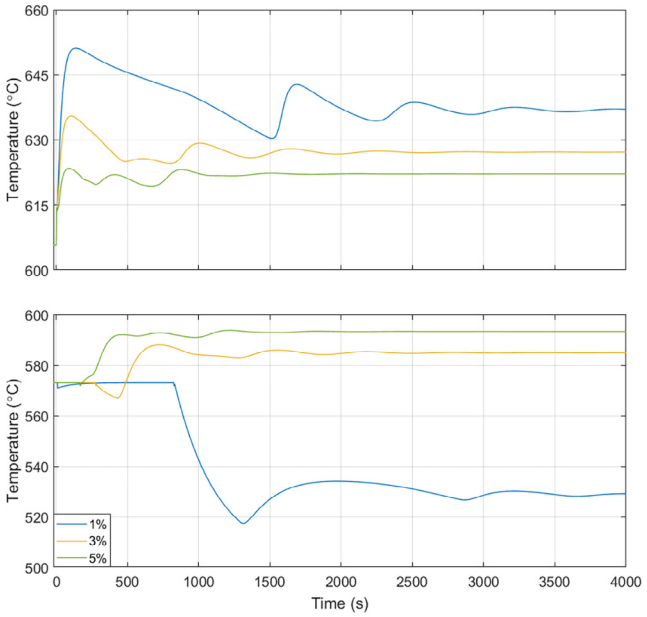

Fig. 21. Coolant salt temperature in the heat exchanger following pump trip in the secondary circuit for different final steady-state thermal convection rates, (a) outlet temperature and (b) inlet temperature.

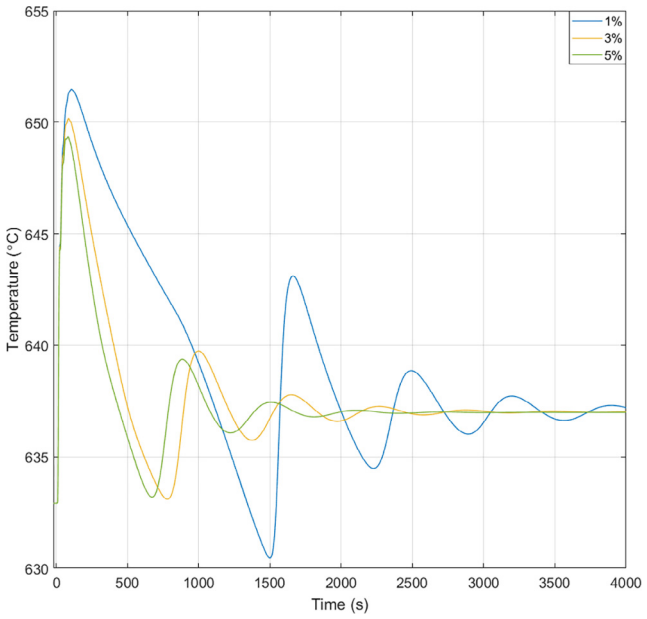

Fig. 23. Average core fuel salt temperatures following pump trip in the secondary circuit for different thermal convection rates of the coolant salt.

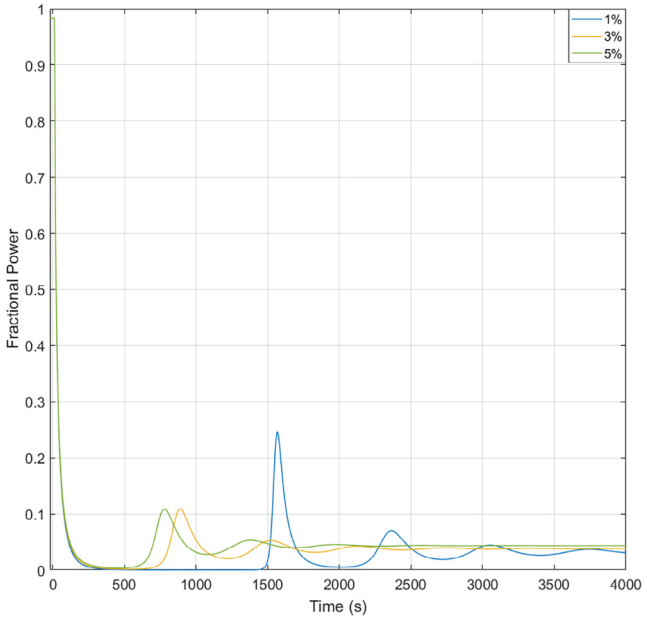

Fig. 22. Response of core power following pump trip in the secondary circuit for different thermal convection rates of the coolant salt.

salt temperature begins to drop for the next several hundred seconds. Meanwhile, "colder" coolant salt from the radiator returning to the heat exchanger further reduces the temperature of the fuel salt. This decrease, in turn, alleviates the negative reactivity feedback suppressing the chain reaction. The power response then shows damped oscillation before settling. Note that both the power and the average core fuel salt temperature settle at similar values for the different final flow rates in the secondary circuit. This is because the heat transfer rate in the secondary system is not very different for the thermal convection rates studied here. Also, the coolant salt does not violate any safety temperature limits in the case of a pump trip in the secondary system. While different coast-down rates for the pump trip in the secondary system were investigated, they did not show any appreciable variation in the system response. Neither was the response noticeably different for the two fuel types.

4.3.3. Cold-slug insertion into the core

Cold-slug incident analysis for a typical light water reactor pertains to pumping colder than normal moderator fluid over the solid fuel. In the case of the MSRE however, the moderator is solid and the fuel is liquid. Thus, for MSRE a cold-slug incident results from introducing a colder than normal mass of fuel salt into the core. Here, the strong negative temperature feedback has the effect of increasing reactivity.

A previous attempt at simulating a cold-slug incident was done by ORNL using MUGATROYD, an IBM-7090 code (Haubenreich and Engel, 1962). Instead of modeling a cold mass in the core, the equivalent reactivity resulting from the temperature change was calculated and introduced. The temperatures listed in Haubenreich and Engel (1962), were averaged between the model and given cold-slug Haubenreich and Engel (1962).

In this study, a cold-slug is simulated by setting the temperature of the fuel entering the core to either 482 °C, 538 °C, or 593 °C using a "switch" function in Simulink. Depending on the duration for which the switch is active, a certain volume of colder salt is introduced into the core. Results from simulations for slug volumes of 0.28 m^3, 0.57 m^3, and 0.85 m^3 are reported here.

The cold-slug causes a reactivity excursion by lowering the average core fuel salt temperature. The power response and average core fuel salt temperature are shown in Fig. 24 for the aforesaid cold-slug temperatures and volumes. In all cases, the average fuel salt temperature initially decreases following the cold-slug insertion until the rise in power brings the fuel salt temperatures back up again. The rising fuel salt temperature then introduces negative feedback damping the power transient. The colder and larger the slug, the bigger the resulting reactivity insertion. Nevertheless, the temperature feedback successfully drives both power and temperature back to nominal values regardless of the volume or temperature of the inserted cold-slug.

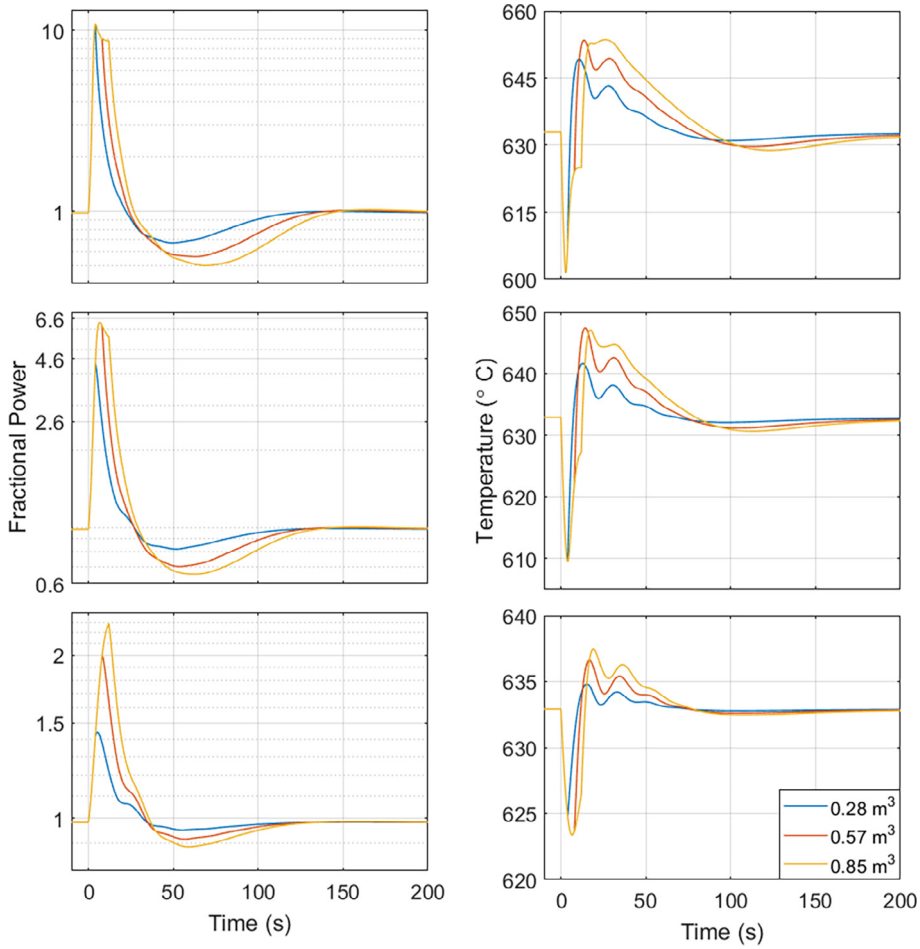

Fig. 24. Power response and average core temperature for different cold-slug volumes at (a) 482 °C (b) 538 °C, and (c) 593 °C.

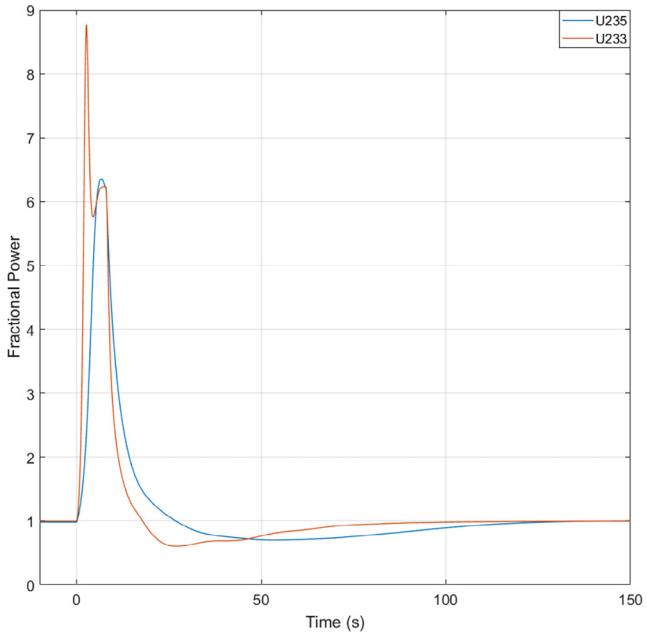

Fig. 25. Comparison of power response for U-233 and U-235 fuel following a cold-slug insertion.

A comparison in the power response following a cold-slug insertion for U-233 and U-235 fuel types is shown in Fig. 25 for a cold-slug volume of 0.57 m^3 at a temperature of 538 °C. The power profiles for the two fuel types are analogous in behavior to the case of an external step insertion. As seen earlier, the U-233 profile shows a higher peak and a secondary peak/plateau in power that is absent for the U-235 case. The reactor power rapidly returns to operational level in both cases.

5. Concluding remarks

As part of the ongoing effort, two nonlinear models have been developed for the MSRE and verified against experimental data. Operational parameters were also assembled for the final version of the MSRE system. The one-region model developed here adopts a simplified core. The nine-region model is an effort to conveniently reproduce the theoretical model elaborated in Ball and Kerlin (1965) and Kerlin et al. (1971b).

The models outlined in this paper are a close approximation of the MSRE. The limitations inherent to the models are:

1. Core neutronics and delayed-neutron precursors are modeled using point kinetics, ignoring spatial effects.
2. Reactivity effects due to xenon poisoning are ignored.

3. Reactivity effects due to circulating void fractions in the fuel salt are ignored.
4. All heat is assumed to be produced in the core.
5. No control action is included.

Simulation results from both models indicate that the MSRE system is stable while operating at all power levels considered. The power and average fuel temperatures show a prompt increase following a reactivity perturbation. At low power levels, the models display a sluggish response as encountered with the power-operated MSRE (Haubenreich and Engel, 1970; Kerlin et al., 1971a; Steffy, 1970). At higher power, the system response is damped due to strong negative reactivity feedback. A "plateau" is seen in the power response for the U-233 fueled case as a consequence of the higher negative reactivity coefficient and lower delayed-neutron fraction. This is comparable to the data published by Kerlin et al. (1971b). The peak in the power response is always lower for the nine-region model due to the importance weighted segmentation of the core. The phase is also slightly different for the two model responses. Both models display a tendency to return to steady-state as was characteristic of the MSRE.

The frequency response generated by the two models compare favorably with the published experimental data for both U-235 and U-233 fuels. The nine-region model essentially reproduces the theoretical modeling results published in Kerlin et al. (1971b). The differences in magnitude and phase encountered between the two models, described above, can be observed clearly in the Bode plots. The general agreement between both models and the published data indicate that the gains from adopting a segmented core model are minimal. While the nine-region model might be more accurate in some cases, the long-term behavior of both models is essentially identical.

Discrepancies were found when comparing experimental results for power response to a step insertion for the cases of 1 MW and 8 MW U-233 fueled MSRE as published in Steffy (1970). The modeling results reported here for these cases match the results published by Guerrieri et al. (2011). For the 1 MW case, the presented models underestimate the experimental data. In the 8 MW case, the models overshoot the experimental data for the given reactivity perturbation. This is further complicated because the models match the data at 5 MW. It was thus ascertained that the experimental data for power response over time as published in Steffy (1970), might be inaccurate. In the absence of the original data logs, there appears to be no resolution to this conundrum.

Simulations of loss-of-flow in the primary loop using the developed one-region model showed that the final thermal convection flow rate in the circuit is the main driver of the power response and temperature profiles. This is due to the circulating delayed-neutron precursors reentering the core faster, and therefore in greater number, at higher final convection rates. The power response showed minute differences for different coast-down rates. The only difference for the two fuel types were the peaks seen in the power response for U-235 fuel due to its higher delayed-neutron fraction.

For the case of secondary pump trip, the average core temperature and power settled at a comparable level regardless of the final convection rate, pump coast-down rate, and fuel type. Cold-slug insertions into the core were found to be analogous to a large reactivity insertion. The feedbacks caused the system to return to nominal power in ~150 s for all the cold-slug volumes and temperatures examined. The difference in behavior following a cold-slug insertion for the two fuel types is akin to the differences seen in their response to a step insertion.

The modeling approach presented here can be extended to study the dynamic behavior of any MSR system with a representative set of parameters. The results discussed in this paper show that simple dynamic models can effectively describe the MSRE behavior. While the nine-region model essentially reproduced the ORNL model, the one-region model matched the available experimental data just as well. Given the general agreement displayed by both models, complicated models may not be necessary to better describe the overall MSRE behavior, though they may have other good uses. Furthermore, the accuracy of some of the available experimental data appears to be problematic.

Given the discussed limitations of experimental data, a substantial effort needs to be devoted to constructing a new experimental molten-salt reactor for MSR technology progress in the 21st century. This reactor could be purpose-built to serve as a test-bed and help provide insights into the intricacies of the reactor dynamics while training a new generation of professionals in developing and operating MSRs.

Acknowledgments

The research and development reported in this paper is supported in part by a grant from Flibe Energy Inc., Huntsville, AL, and by the U.S. Nuclear Regulatory Commission graduate fellowship, under contract with the University of Tennessee. The authors are grateful to Dr. Tom Kerlin, Professor Emeritus of Nuclear Engineering, University of Tennessee, for the technical discussion about molten salt reactors.

Conflict of interest statement

The authors declare that there is no conflict of interest.

Appendix A

Table A1
Modeling parameters (Robertson, 1965; Kerlin et al., 1971; Haubenreich et al., 1964; Ball and Kerlin, 1965; Steffy, 1970).

Nominal power	8 MW(th)
Fraction of power generated in the salt	0.93
Fraction of power generated in the graphite	0.07
Mass of salt in core	1374 kg
Mass of graphite in core	3634 kg
Mass flow rate in the primary circuit	162 kg/s
Mass flow rate in the secondary circuit	100 kg/s
Specific heat capacity of fuel salt	1966 J kg^{-1} $°C^{-1}$
Specific heat capacity of graphite	1773 J kg^{-1} $°C^{-1}$
Specific heat capacity of coolant salt	2390 J kg^{-1} $°C^{-1}$
Mass of fuel salt in the heat exchanger	348 kg
Mass of coolant salt in the heat exchanger	100 kg
Heat transfer coefficient between fuel and graphite	0.036 MW $°C^{-1}$
Heat transfer coefficient between fuel salt and metal	0.648 MW $°C^{-1}$
Heat transfer coefficient between coolant salt and metal	0.306 MW $°C^{-1}$
Core inlet temperature	632 °C
Core outlet temperature (nominal power)	657 °C
Heat exchanger inlet temperature for coolant salt	546 °C
Heat exchanger outlet temperature for coolant salt	579 °C
Time delay – core to heat exchanger	3.77 s
Time delay – heat exchanger to core	8.67 s
Time delay – heat exchanger to radiator	4.71 s
Time delay – radiator to heat exchanger	8.24 s

Table A2
Parameters for nine-region core (Ball and Kerlin, 1965).

Region	τ_{f1}	τ_{f2}	K_1	K_2	K_{g1}	K_{g2}
1	1.386	1.454	0.01493	0.01721	0.000946	0.001081
2	2.083	1.424	0.02736	0.04550	0.001685	0.003060
3	1.139	1.139	0.04504	0.04656	0.003029	0.003131
4	1.424	2.772	0.05126	0.04261	0.003447	0.002395
5	2.084	1.424	0.03601	0.06069	0.002216	0.004081
6	1.139	1.139	0.06014	0.06218	0.004044	0.004182
7	1.424	2.774	0.06845	0.05664	0.004603	0.003184
8	2.371	1.380	0.06179	0.07707	0.003920	0.005183
9	1.610	2.700	0.09333	0.07311	0.006277	0.004305

Region	MC_{p1} (MJ °C^{-1})	MC_{p2} (MJ °C^{-1})	MC_{pg} (MJ °C^{-1})	hA (MW °C^{-1})	I_{f1}	I_{f2}	I_g
1	0.02718	0.02844	0.12600	0.0007056	0.02168	0.02678	0.04443
2	0.09216	0.06282	0.38052	0.0021672	0.02197	0.06519	0.08835
3	0.05040	0.05040	0.28908	0.0016200	0.07897	0.08438	0.16671
4	0.06300	0.12276	0.37008	0.0021132	0.08249	0.04124	0.12077
5	0.15588	0.10656	0.64368	0.0035586	0.02254	0.06801	0.09181
6	0.08514	0.08514	0.48924	0.0027450	0.08255	0.08823	0.17429
7	0.10656	0.20736	0.62604	0.0035730	0.08623	0.04290	0.12612
8	0.4284	0.24912	1.73016	0.0098010	0.02745	0.05529	0.08408
9	0.2907	0.4878	1.69578	0.0096480	0.06936	0.03473	0.10343

References

Ball, S.J., Kerlin, T.W., 1965. *Stability Analysis of the Molten Salt Reactor Experiment*, ORNL-TM-1070. Oak Ridge National Laboratory.

Burke, O.W., 1960. MSRE Analog Computer Simulation of a Loss-of-Flow Accident in the Secondary System, ORNL-CF-11-20. Oak Ridge National Laboratory.

Cammi, A., Fiorina, C., Guerrieri, C., Luzzi, L., 2012. Dimensional effects in the modelling of MSR dynamics: moving on from simplified schemes of analysis to a multiphysics modelling approach. Nucl. Eng. Des. 246, 12–26.

Documents Related to Liquid-Halide (Fluoride and Chloride) Reactor Research and Development, Web archive https://www.energyfromthorium.com/pdf.

Guerrieri, C., Cammi, A., Fiorina, C., Luzzi, L. Preliminary assessment of modelling issues related to the dynamics and control of MSRs. In: Proceedings of the International Congress for Advanced Power-Plants, Paper 11099, Nice, France, 2011.

Haubenreich, P.N., Engel, J.R., 1962. *Safety Calculations for MSRE*, ORNL-TM-0251. Oak Ridge National Laboratory.

Haubenreich, P.N., Engel, J.R., 1970. Experience with the molten-salt reactor experiment. Nucl. Appl. Technol. 8 (2), 118–136.

Haubenreich, P.N., Engel, J.R., Prince, B.E., Claiborne, H.C., 1964. MSRE Design and Operations Report, Part III. Nuclear Analysis, ORNL-TM-0730. Oak Ridge National Laboratory.

Kerlin, T.W., Ball, S.J., 1966. Experimental Dynamic Analysis of the Molten-Salt Reactor Experiment, ORNL-TM-1647. Oak Ridge National Laboratory.

Kerlin, T.W., Ball, S.J., Steffy, R.C., 1971b. Theoretical dynamic analysis of the molten-salt reactor experiment. Nucl. Technol. 10, 118–132.

Kerlin, T.W., Ball, S.J., Steffy, R.C., Buckner, M.R., 1971a. Experiences with dynamic testing methods at the molten-salt reactor experiment. Nucl. Technol. 10, 103–117.

Klee, H., Allen, R., 2011. Simulation of Dynamic Systems with MATLAB and SIMULINK. CRC Press, Boca Raton.

Lindauer, R.B., 1969. Processing of the MSRE Flush and Fuel Salts, ORNL-TM-2578. Oak Ridge National Laboratory.

MacPherson, H.G., 1960. Molten-Salt Reactor Program: Quarterly Progress Report for Period Ending July 31, 1960, ORNL-3014. Oak Ridge National Laboratory.

McNeese, L.E., 1976. Molten-Salt Reactor Program Semiannual Progress Report for Period Ending February 29, 1976, ORNL-5132. Oak Ridge National Laboratory.

Robertson, R.C., 1965. MSRE Design and Operations Report Part I: Description of Reactor Design, ORNL-TM-0728. Oak Ridge National Laboratory.

Rohatgi, A. WebPlotDigitizer version 3.12, Web app https://arohatgi.info/WebPlotDigitizer.

Rosenthal, M.W., 2009. An Account of Oak Ridge National Laboratory's Thirteen Nuclear Reactors, ORNL-TM-2009. Oak Ridge National Laboratory.

Singh, V., Lish, M.R., Chvála, O., Upadhyaya, B.R., 2017a. Dynamics and control of molten-salt breeder reactor. Nucl. Eng. Technol. 49, 887–895.

Singh, V., Lish, M.R., Chvála, O., Upadhyaya, B.R., 2017b. Dynamic modeling and performance analysis of a two-fluid molten-salt breeder reactor system. Nucl. Technol.

Steffy Jr., R.C., Wood, P.J., 1969. Theoretical Dynamic Analysis of MSRE with ^{233}U Fuel, ORNL-TM-2571,. Oak Ridge National Laboratory.

Steffy Jr., R.C., 1970. Experimental Dynamic Analysis of MSRE with ^{233}U Fuel, ORNL-TM-2997. Oak Ridge National Laboratory.